Nonlinear atmospheric teleconnections

William W. Hsieh,[1] Aiming Wu,[1] and Amir Shabbar[2]

Neural network models are used to reveal the nonlinear winter atmospheric teleconnection patterns associated with the El Niño-Southern Oscillation (ENSO) and with the Arctic Oscillation (AO) over the N. Hemisphere. The nonlinear teleconnections (for surface air temperature, precipitation, sea level pressure and 500 hPa geopotential height) are found to relate quadratically to the ENSO and AO indices. Relative to linear teleconnections, nonlinear teleconections appear to propagate perturbations farther, into regions where classical linear teleconnections are insignificant.

1. Introduction

Contemporaneous correlations between distant atmospheric variables, commonly referred to as teleconnections, reveal the propagation of perturbations over vast distances via the atmosphere. The El Niño-Southern Oscillation (ENSO) [*McPhaden*, 2004] in the tropical Pacific tends to excite the Pacific/North American (PNA) atmospheric teleconnection pattern [*Horel and Wallace*, 1981; *Wallace and Gutzler*, 1981] in winter. Another N. Hemisphere winter teleconnection pattern which lies mainly over the Arctic and North Atlantic is the North Atlantic Oscillation (NAO), also referred to as the Arctic Oscillation (AO) [*Thompson and Wallace*, 1998].

In recent years, the asymmetry between the warm and cold states of ENSO in the tropical Pacific, and the corresponding asymmetry in the extratropical winter teleconnection have been studied, mainly by composite methods [*Hoerling et al.*, 1997; *Lin and Derome*, 2004]. Neural network (NN) models [*Hsieh*, 2004; *Hsieh and Tang*, 1998] offer potentially more powerful tools to extract nonlinear signals. In particular, linear projection (LP) [*Deser and Blackmon*, 1995] has been generalized to nonlinear projection (NLP) using NN [*Wu and Hsieh*, 2004a, 2004b; *Wu et al.*, 2005], where an ENSO or AO index x is nonlinearly projected onto the winter extratropical N. Hemisphere climate anomaly variables $\mathbf{y}$. The least squares fit $\mathbf{y} = \mathbf{f}(x)$ is performed, with the nonlinear mapping functions $\mathbf{f}$ given by the NN model.

Our previous studies have only examined the NLP applied to individual fields or separate geographic regions. In this paper, we interconnect 4 variables — sea level pressure (SLP), surface air temperature (SAT), 500 hPa geopotential height (Z500), and standardized precipitation (PRCP) — over the whole N. Hemisphere, and we compare the nonlinear teleconnections of ENSO and AO.

---

[1]Department of Earth and Ocean Sciences, University of British Columbia, Vancouver, B.C., Canada

[2]Meteorological Service of Canada, Toronto, Ont., Canada

2. Data and Methods

The winter (November to March) data used were monthly data from 1948-2002, 20°N-90°N, with the $0.5° \times 0.5°$ resolution land SAT and PRCP from the Climate Research Unit of the Univ. of East Anglia, the $5° \times 5°$ resolution SLP from the National Center for Atmospheric Research (NCAR) [*Trenberth and Paolino*, 1980] and the $2.5° \times 2.5°$ Z500 from the National Centers for Environment Prediction (NCEP) reanalysis [*Kalnay*, 1996]. Anomalies were obtained by subtracting the climatological seasonal cycle. Only the leading 10 SLP, 10 Z500, 12 SAT and 13 PRCP principal components (PC) were retained, containing, respectively, 86, 81, 79 and 51% of the variance. The AO index is the standardized leading PC of the winter SLP anomalies, while the ENSO index is the leading PC of the winter sea surface temperature (SST) anomalies over the tropical Pacific (20°S-20°N, 122°E-80°W) (using the $2° \times 2°$ ERSST2 dataset from the National Climate Data Center, NOAA).

LP is simply linear regression with a single input (predictor) x (the ENSO or AO index) mapped to the output $\mathbf{y}$ (the leading PCs of an atmospheric anomaly field), with no time lag. NLP is performed using a multi-layer perceptron NN model [*Bishop*, 1995] with a single hidden layer (containing intermediate variables h_i, $i = 1, \ldots, m$), so the mapping is $x \to \mathbf{h} \to \mathbf{y}$, with

$$h_i = \tanh(w_i x + b_i), \quad y_j = \sum_i W_{ji} h_i + a_j, \quad (1)$$

where the model parameters $\mathbf{w}$, $\mathbf{b}$, $\mathbf{W}$ and $\mathbf{a}$ are determined by minimizing the mean square error (MSE) of $\mathbf{y}$. With large enough m, the NN is capable of modelling any nonlinear continuous function $\mathbf{y} = \mathbf{f}(x)$ to arbitrary accuracy [*Bishop*, 1995]. To avoid local minima during the optimization, the NN model was trained 30 times with random initial parameters, with the smallest MSE solution selected. To reduce sampling dependence, we repeated the process 400 times, where each bootstrap [*Efron and Tibshirani*, 1993] sample was obtained by randomly selecting (with replacement) one winter's data record 55 times from the original record of 55 winters. The ensemble mean of the resulting 400 NN models was used as the final model for the NLP. The final model was run with $m = 3$, after sensitivity tests showed the final model to be insensitive to m ranging from 2 to 5. More details of our methodology are given in *Wu and Hsieh* [2004b].

3. Results

Though projections were made separately onto the winter N. Hemisphere SLP anomalies, SAT anomalies, Z500 anomalies, and PRCP anomalies from the ENSO and the AO index, overlaying different variables in plots would reveal interconnections. With $\mathbf{f}$ nonlinear, the $\mathbf{y}$ pattern associated with a fluctuating x is not given by a standing wave pattern, but changes continuously with x, and can only be viewed via videos, with supporting Video 1 [1] showing the LP and NLP from the ENSO index onto the SLP, SAT, Z500 and PRCP anomalies, and Video 2 projecting from the AO index. The NLP solution can be decomposed into a linear and a nonlinear component. The linear component is simply LP, while the nonlinear component is NLP−LP. Applying principal component analysis (PCA) to this nonlinear component [*Wu and Hsieh*, 2004b] yields a first mode containing over 99% of the variance (where the high percentage variance results

from NLP−LP being a noiseless map from a single degree of freedom given by the ENSO or AO index). The PCA spatial pattern displays the nonlinear teleconnection pattern for ENSO (Figures 1b and f), while the patterns from the linear component (Figures 1a and e) give the familiar linear teleconnection patterns. The PCs of the nonlinear component of SAT (Figure 1c) and SLP are very similar to one another, and are essentially a quadratic response to the ENSO index (as verified by a polynomial fit). Thus the PCs take on large positive values whenever the ENSO index indicates a warm or a cold episode. The time-varying anomaly field is the product of the PCA spatial pattern in Figure 1b and the corresponding PC time series, hence the pattern in Figure 1b is excited during both warm and cold ENSO episodes. In both Figures 1a and b, the anomalies in the SAT are generally consistent with the interpretation that regions of positive and negative SLP anomalies have, respectively, anomalous clockwise and anticlockwise circulation anomalies, and airflow from the south or the ocean raises the SAT while airflow from the north or from land lowers the SAT.

For the PRCP and Z500 anomalies, the PCs of their nonlinear components are also quadratically related to the ENSO index (Figure 1d). The nonlinear teleconnection pattern of the PRCP anomalies (Figure 1f) are generally consistent with the circulation patterns associated with the Z500 anomaly pattern (Figure 1f), with airflow from the ocean or from the south raising the PRCP, and airflow from land or from the north lowering the PRCP. Most strikingly, while the linear teleconnection patterns of the 4 variables (Figures 1a and e) are mainly concentrated in the North Pacific and western North America, the nonlinear teleconnection patterns (Figures 1b and 1f) reveal strong signals in the Europe-North Atlantic-eastern North America region. In particular, in this region, the presence of negative SLP and Z500 anomalies at high latitudes and positive anomalies at mid latitudes means that the positive phase of the NAO is excited during both warm and cold ENSO episodes. Averaged over the N. Hemisphere (20°N-90°N), the variance contributed by the nonlinear component of the NLP for SLP, Z500, SAT and PRCP is, respectively, 34, 33, 30 and 42% that of the linear component.

The corresponding results for the NLP of the AO index onto the winter N. Hemisphere (Figure 2) also reveal nonlinear teleconnection patterns (Figures 2b and f), though relative to the linear teleconnection patterns (Figures 2a and 2e), they are not manifested as strongly as in the case of ENSO (Figure 1). Again the PCs of the nonlinear component show that they are basically quadratically related to the AO index (Figures 2c and d). The nonlinear teleconnection patterns for SAT (Figure 2b) and PRCP (Figure 2f) are again generally consistent with the circulation anomalies associated with the nonlinear teleconnection patterns of the SLP and Z500. While the linear teleconnection patterns for the AO (Figures 2a and e) are focused on the Arctic-N.Atlantic-Europe region, the nonlinear patterns are relatively strong outside this region, manifesting strength in the N. Pacific and western N. America. Averaged over the N. Hemisphere, the variance of the nonlinear component of the NLP for SLP, Z500, SAT and PRCP is, respectively, 3, 3, 4 and 14% that of the linear component. Thus nonlinear teleconnection of AO is much weaker than that of ENSO. The nonlinear teleconnection patterns in Figures 1 and 2 are statistically significant at the 5% level, based on the bootstrap distributions.

4. Conclusion and Discussion

As the main region of ENSO activity is in the Pacific, while that of AO is in the N. Atlantic sector, it is remarkable that the nonlinear teleconnection effects from ENSO extend strongly into the N. Atlantic sector, and those from AO into the N. Pacific region. This suggests that the mechanism for nonlinear teleconnection allows farther propagation from the source region than that for linear teleconnection. The exact mechanism for nonlinear teleconnection is not clear; however, as anomalous winds $\mathbf{u}'$ and temperatures T' are expected to reverse sign as the ENSO or AO index reverses, the presence of quadratic terms like $\mathbf{u}' \cdot \nabla \mathbf{u}'$ and $\mathbf{u}' \cdot \nabla T'$ in the governing equations provides a possible explanation as to why the nonlinear response is mainly quadratic with respect to the ENSO or AO index. In the tropical Pacific, $\mathbf{u}' \cdot \nabla T'$ is important in producing nonlinear ENSO structures [*An and Jin*, 2004].

Since the nonlinear behavior is predominantly quadratic, we have found that the quadratic polynomial fit, i.e. $\mathbf{y} = \mathbf{a}_1 x + \mathbf{a}_2 x^2 + \mathbf{a}_0$, gives spatial patterns of $\mathbf{a}_2$ [*Wu and Hsieh*, 2004b] which are similar to the nonlinear teleconnections patterns in Figures 1 and 2 from NN. For extratropical seasonal climate predictions [*Shabbar and Barnston*, 1996], incorporating nonlinear teleconnections may lead to enhanced forecast skills, especially in regions where the classical linear teleconnections are weak but the nonlinear teleconnections are not.

Notes

1. Supporting material is available via Web browser or via Anonymous FTP from ftp://ftp.agu.org/apend/" (Username = "anonymous", Password = "guest").
Subdirectories in the ftp site are arranged by journal and paper number. Information on searching and submitting electronic supplements is found at http://www.agu.org/pubs/esupp_about.html

References

An, S.-I., and F.-F. Jin (2004), Nonlinearity and asymmetry of ENSO, *J. Clim.*, *17*, 2399-2412.

Bishop, C. M. (1995), *Neural Networks for Pattern Recognition*, 482 pp., Clarendon Pr., Oxford.

Deser, C., and M. L. Blackmon (1995), On the relationship between tropical and North Pacific sea surface temperature variations, *J. Clim.*, *8*, 1677-1680.

Efron, B., and R. J. Tibshirani (1993), *An Introduction to the Bootstrap*, 436 pp., CRC Press, Boca Raton, Florida.

Hoerling, M. P., A. Kumar, and M. Zhong (1997), El Niño, La Niña and the nonlinearity of their teleconnections, *J. Clim.*, *10*, 1769-1786.

Horel, J. D., and J. M. Wallace (1981), Planetary-scale atmospheric phenomena associated with the Southern Oscillation, *Mon. Weath. Rev.*, *109*, 813-829.

Hsieh, W. W. (2004), Nonlinear multivariate and time series analysis by neural network methods, *Rev. Geophys.*, *42*, RG1003, doi:1010.1029/2002RG000112.

Hsieh, W. W., and B. Tang (1998), Applying neural network models to prediction and data analysis in meteorology and oceanography, *Bull. Am. Meteorol. Soc.*, *79*, 1855-1870.

Lin, H., and J. Derome (2004), Nonlinearity of the extratropical response to tropical forcing, *J. Clim.*, *17*, 2597-2608.

McPhaden, M. J. (2004), Evolution of the 2002-03 El Niño, *Bull. Am. Meteorol. Soc.*, *85*, 677-695.

Shabbar, A., and A. G. Barnston (1996), Skill of seasonal climate forecasts in Canada using Canonical Correlation Analysis, *Mon. Weath. Rev.*, *124*, 2370-2385.

Thompson, D. W. J., and J. M. Wallace (1998), The Arctic Oscillation signature in the wintertime geopotential height and temperature fields., *Geophys. Res. Lett.*, *25*, 1297-1300.

Wallace, J. M., and D. S. Gutzler (1981), Teleconnections in the geopotential height fields during the northern hemisphere winter, *Mon. Weath. Rev.*, *109*, 784-812.

Wu, A., and W. W. Hsieh (2004a), The nonlinear association between ENSO and the Euro-Atlantic winter sea level pressure, *Clim. Dynam.*, *23*, 859-868.

Wu, A., and W. W. Hsieh (2004b), The nonlinear Northern Hemisphere atmospheric response to ENSO., *Geophys. Res. Lett.*, *31*, L02203, doi:02210.01029/02003GL018885.

Wu, A., W. W. Hsieh, and A. Shabbar (2005), The nonlinear patterns of North American winter temperature and precipitation associated with ENSO., *J. Clim.*, *18*, 1736-1752. doi: 1710.1175/JCLI3372.1731.

William W. Hsieh, Department of Earth and Ocean Sciences, University of British Columbia, 6339 Stores Road, Vancouver, B.C. V6T 1Z4, Canada. (whsieh@eos.ubc.ca)
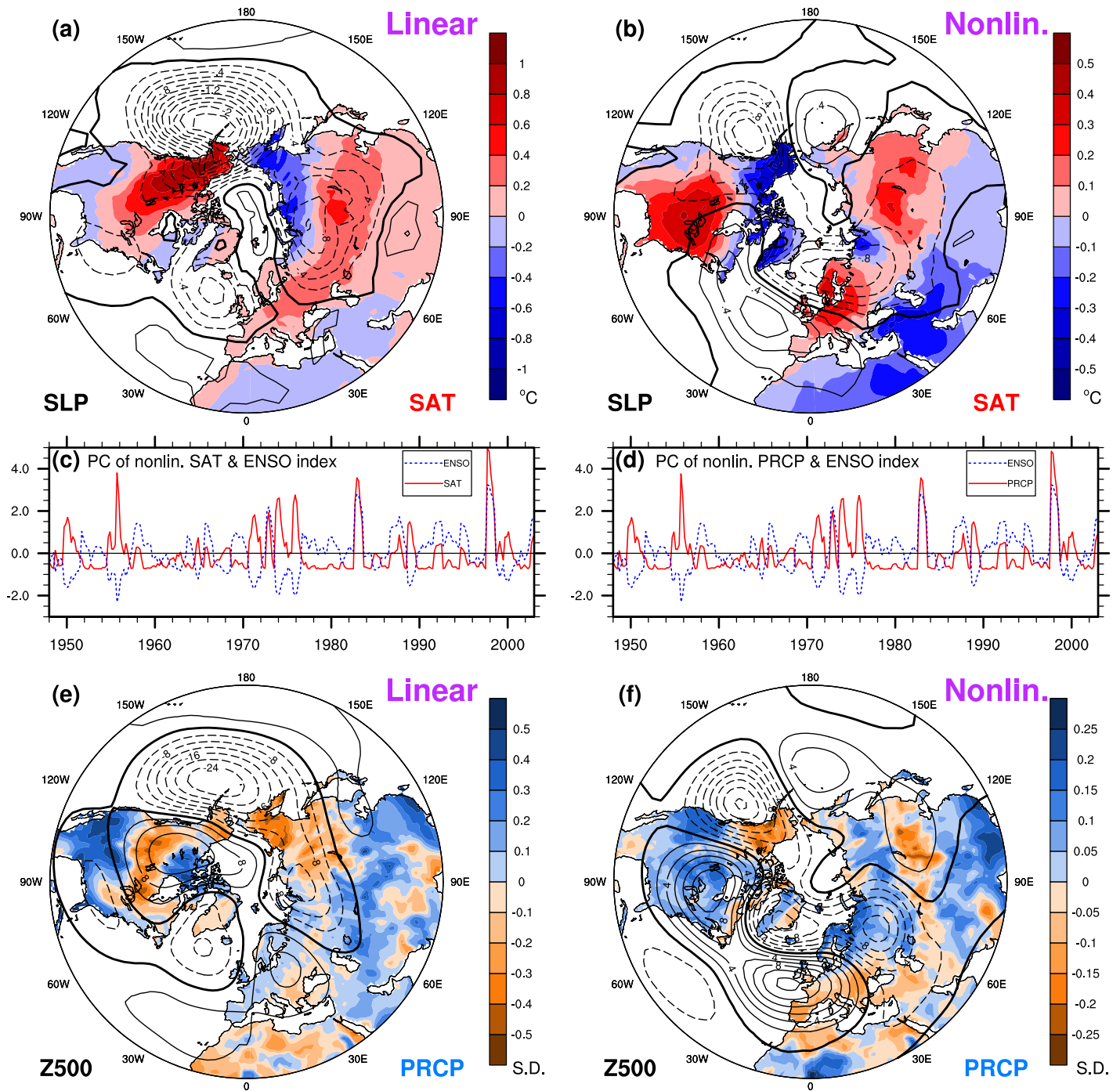
Figure 1. Spatial patterns for the (a) linear and (b) nonlinear components of the NLP model projecting from the ENSO index (with zero time lag) onto the winter SAT (°C) (colored) anomalies and the SLP (hPa) (contoured) anomalies, with the solid, dashed and thick contours representing positive, negative and zero values, respectively. In (c), the PC associated with the SAT pattern in (b), and the ENSO index (dashed) are shown. The PC for the SLP pattern, if plotted, would basically overlap with the PC of the SAT (as their correlation exceeds 0.99). The linear and nonlinear patterns for PRCP (colored) and Z500 (m) (contoured) are shown in (e) and (f) respectively, and the PC for the nonlinear component of PRCP in (d). The PC for Z500, if drawn, would basically overlap with the PC of PRCP (correlation over 0.98).
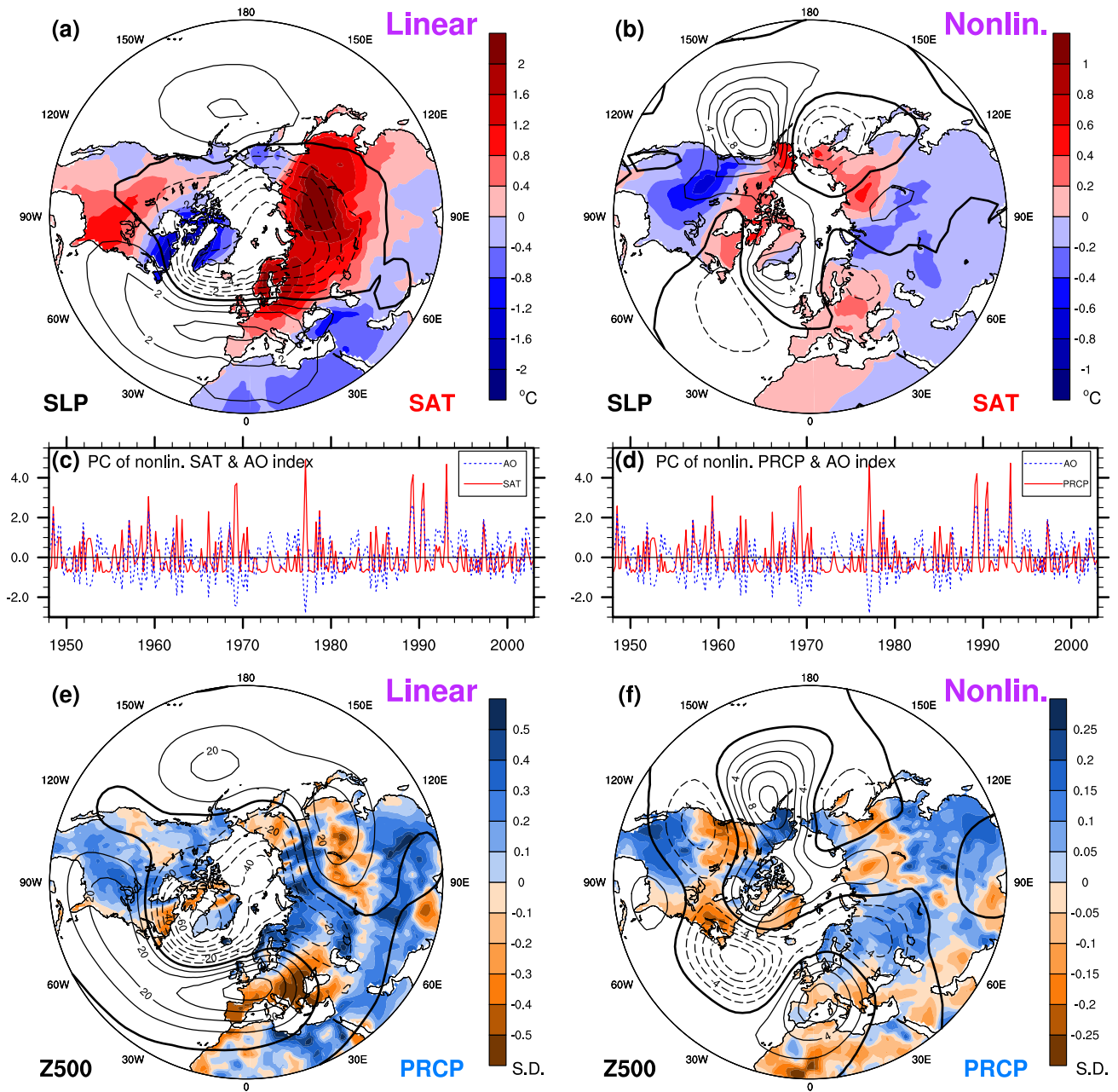
Figure 2. Spatial patterns for the (a) linear and (b) nonlinear components of the NLP model projecting from the AO index onto the winter SAT (colored) anomalies and the SLP (contoured) anomalies. In (c), the PC of the SAT pattern in (b), and the AO index (dashed) are shown. The PC of SLP, if drawn, would basically overlap with the PC of SAT (correlation over 0.99). The linear and nonlinear patterns for PRCP (colored) and Z500 (contoured) are shown in (e) and (f) respectively, and the PC for the nonlinear component of PRCP in (d). The PC of Z500 would basically overlap with the PC of SAT (correlation over 0.99).